J|A|C|S
ARTICLES
Published on Web 06/13/2003

Photoisomerization and Proton Transfer in Photoactive Yellow Protein

Michael J. Thompson, Donald Bashford,* Louis Noodleman,* and Elizabeth D. Getzoff*

Department of Molecular Biology, MB4, Skaggs Institute for Chemical Biology, The Scripps Research Institute, 10550 N. Torrey Pines Rd., La Jolla, California 92037

Received November 22, 2002; E-mail: bashford@scripps.edu; lou@scripps.edu; edg@scripps.edu

Abstract: The photoactive yellow protein (PYP) is a bacterial photosensor containing a *para*-coumaryl thioester chromophore that absorbs blue light, initiating a photocycle involving a series of conformational changes. Here, we present computational studies to resolve uncertainties and controversies concerning the correspondence between atomic structures and spectroscopic measurements on early photocycle intermediates. The initial nanoseconds of the PYP photocycle are examined using time-dependent density functional theory (TDDFT) to calculate the energy profiles for chromophore photoisomerization and proton transfer, and to calculate excitation energies to identify photocycle intermediates. The calculated potential energy surface for photoisomerization matches key, experimentally determined, spectral parameters. The calculated excitation energy of the photocycle intermediate cryogenically trapped in a crystal structure by Genick et al. [Genick, U. K.; Soltis, S. M.; Kuhn, P.; Canestrelli, I. L.; Getzoff, E. D. *Nature* **1998**, *392*, 206−209] supports its assignment to the PYP_B (I_0) intermediate. Differences between the time-resolved room temperature (298 K) spectrum of the PYP_B intermediate and its low temperature (77 K) absorbance are attributed to a predominantly deprotonated chromophore in the former and protonated chromophore in the latter. This contrasts with the widely held belief that chromophore protonation does not occur until after the PYP_L (I_1 or pR) intermediate. The structure of the chromophore in the PYP_L intermediate is determined computationally and shown to be deprotonated, in agreement with experiment. Calculations based on our PYP_B and PYP_L models lead to insights concerning the PYP_{BL} intermediate, observed only at low temperature. The results suggest that the proton is more mobile between Glu46 and the chromophore than previously realized. The findings presented here provide an example of the insights that theoretical studies can contribute to a unified analysis of experimental structures and spectra.

1 Introduction

Many photosensory proteins transduce the energy of an absorbed photon into a signal to initiate a cellular response via a photocycle, which is a sequence of coupled electronic and conformational changes in a protein−chromophore system. Newly developed time-resolved and cryogenic trapping techniques in both spectroscopy and structural biology have generated a wealth of data about the function of photoactive proteins and the nature of their photocycle intermediates. However, coupling the results from these diverse techniques to develop a coherent picture of protein function remains a challenge. Here, we use quantum chemical calculations to resolve questions from experimental photobiology.

The photoactive yellow protein (PYP) is among the most well-characterized photosensors. Its small size (14 kD), high thermal stability and water solubility, and the similarity of its photocycle with the bacterial rhodopsins,[1−3] make it an attractive model system for biological photosensing. PYP exists in several halophilic purple bacteria,[4−6] where it is thought to serve as the photosensor initiating negative phototactic response to blue light.[7] PYP's chromophore, *p*-coumaric acid, is attached via a thioester linkage to the only cysteine residue in the protein (Cys69).[2,8,9] In the dark state of the photocycle, the chromophore is in the trans conformation[9] and is deprotonated.[8−11] The buried charge on the chromophore is stabilized by hydrogen bonds from Tyr42 and Glu46 (protonated) to its phenolate oxygen (Figure 1a), and from the peptide backbone to its carbonyl oxygen (not shown).[9] Following the absorption of blue light (λ_{max} = 446

(1) Meyer, T. E.; Yakali, E.; Cusanovich, M. A.; Tollin, G. *Biochemistry* **1987**, *26*, 418.
(2) Hoff, W. D.; Dux, P.; Hard, K.; Devreese, B.; Nugteren-Roodzant, I. M.; Crielaard, W.; Boelens, R.; Kaptein, R.; van Beeumen., J.; Hellingwerf, K. J. *Biochemistry* **1994**, *33*, 13 959.
(3) Hellingwerf, K. J.; Hoff, W. D.; Crielaard, W. *Mol. Microbiol.* **1996**, *21*, 683.
(4) Meyer, T. E. *Biochim. Biophys. Acta* **1985**, *806*, 175.
(5) Meyer, T. E.; Tollin, G.; Causgrove, T. P.; Cheng, P.; Blankenship, R. E. *Biophys. J.* **1991**, *59*, 988.
(6) Koh, M.; Van Driessche., G.; Samyn, B.; Hoff, W. D.; Meyer, T. E.; Cusanovich, M. A.; Van Beeumen., J. J. *Biochemistry* **1996**, *35*, 2526.
(7) Sprenger, W. W.; Hoff, W. D.; Armitage, J. P.; Hellingwerf, K. J. *J. Bacteriol.* **1993**, *175*, 3096.
(8) Baca, M.; Borgstahl, G. E.; Boissinot, M.; Burke, P. M.; Williams, D. R.; Slater, K. A.; Getzoff, E. D. *Biochemistry* **1994**, *33*, 14369.
(9) Borgstahl, G. E.; Williams, D. R.; Getzoff, E. D. *Biochemistry* **1995**, *34*, 6278.
(10) Kim, M.; Mathies, R. A.; Hoff, W. D.; Hellingwerf, K. J. *Biochemistry* **1995**, *34*, 12669.
(11) Demchuk, E.; Genick, U. K.; Woo, T. T.; Getzoff, E. D.; Bashford, D. *Biochemistry* **2000**, *39*, 1100.

10.1021/ja0294461 CCC: $25.00

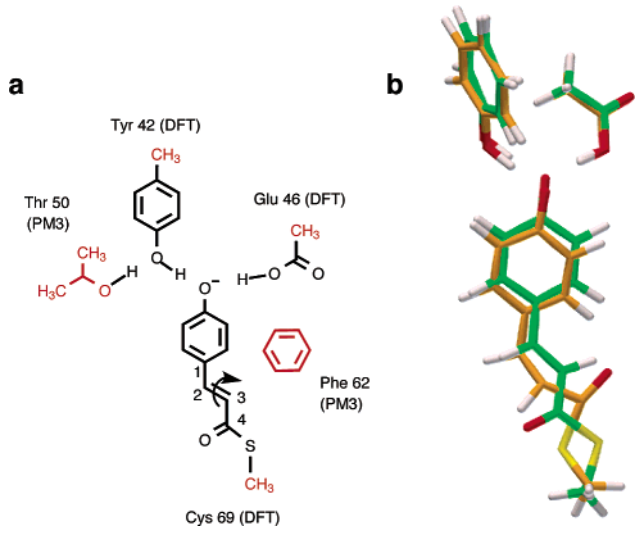

Figure 1. PYP active site models examined in this study. (a) Model used in photoisomerization energy surface determination, where $\theta(C_4C_3C_2C_1)$ is the isomerizing bond. Functional groups in red are constrained to their positions in the dark state protein conformation.[12] Level of theoretical description in the ONIOM calculation is shown in parentheses (DFT or PM3). (b) Two photocycle intermediates observed as dual conformations with partial occupancy in the single-crystal structure of Genick et al.[12] The dark state (green carbon atoms) and light-exposed cryogenically trapped intermediate (orange carbon atoms) models are used to calculate excitation energies and proton-transfer energy surfaces.

nm), PYP undergoes a photocycle involving both trans → cis isomerization and protonation of its chromophore. The protein structural changes are presumed to modulate interactions with an as-yet-unknown factor in the signaling pathway.

Progress toward understanding the PYP photocycle has been made through coupling extensive studies using both time-resolved techniques and cryogenic trapping of intermediates monitored by UV−vis spectroscopy,[13−18] IR−Raman spectroscopy,[19−22] and X-ray crystallography.[12,23,24] Following absorption of blue light by the anionic chromophore in the dark state, PYP_G (also called P or pG), a series of photocycle intermediates is observed by time-resolved spectroscopy (Figures 2a,c). The chromophore relaxes back to the ground state potential energy surface resulting in the formation of one or more early intermediates within the first few picoseconds.[16] This early intermediate stage has been analyzed in terms of proposed states PYP_B and PYP_H[14] (Figure 2a) or in terms of proposed states I_0 and $I_0^{\ddagger}$[15] (Figure 2c). Next, the PYP_L (456 nm; also called I_1 or pR) intermediate is formed on the nanosecond time scale. Vibrational spectroscopy[20] shows that the hydrogen bond between the deprotonated chromophore and the protonated Glu46 observed in the dark state intermediate is maintained in the PYP_L intermediate. In the PYP_L intermediate, the cis conformation of the vinyl bond of the chromophore results from flipping of the carbonyl oxygen along with its thioester linkage to the protein.[12,21,23] The PYP_L intermediate relaxes to PYP_M ($\tau \cong 100$ μs; also called I_2 or pB), the putative signaling intermediate. The chromophore of PYP_M is in the cis conformation, but differs in that the phenolic oxygen of the chromophore is solvent exposed and protonated while the resting state hydrogen bonding network is broken.[21,24,25] Protonation of the chromophore between the PYP_L and PYP_M intermediates is expected to occur by proton transfer from Glu46[20,26−28] or alternatively from solvent.[20,29,30] The PYP_M intermediate relaxes back to the dark state ($\tau = 140$ ms) by both deprotonating and re-isomerizing from cis → trans in a less understood, pH-dependent "back-reaction".[11,24,31]

Cryogenic trapping techniques have been used to gain insight into the nature of the early photocycle intermediates (Figure 2b). The approach uses temperatures low enough to prevent thermal crossing of activation barriers between intermediates, thereby isolating particular states for characterization with methods of lower time resolution. Light excitation of the protein cryo-cooled in liquid nitrogen (77 K) gives a mixture of two intermediates, PYP_B ($\lambda_{max} = 489$ nm)[13,32] and PYP_H (442 nm).[13] The difference in λ_{max} of the PYP_B intermediate between the room temperature (509 nm) and low temperature (489 nm) has not been explained, but the results presented here suggest the difference is due to protonation of the chromophore. Two additional thermal products of PYP_B and PYP_H, identified as PYP_{BL} (400 nm) and PYP_{HL} (447 nm) respectively, are observed only at low temperature.[13] The PYP_L intermediate isolated at low temperature has properties similar to those observed at room temperature.[19−22] Warming of the cryogenically trapped PYP_L intermediate results in return to the dark state without cryogenic isolation of PYP_M,[13] completing the photocycle.

In this study, we use quantum chemical calculations to evaluate the energetics of both photoisomerization of the central vinyl bond, $\theta(C_4C_3C_2C_1)$, of the PYP chromophore, and proton transfer from Glu46 to the chromophore (Figure 1a). The primary objective of this paper is to present the assignment of both crystallographically and computationally determined atomic structures to several subpicosecond to nanosecond photocycle intermediates. This is accomplished by comparing calculated

(12) Genick, U. K.; Soltis, S. M.; Kuhn, P.; Canestrelli, I. L.; Getzoff, E. D. *Nature* **1998**, *392*, 206.
(13) Imamoto, Y.; Kataoka, M.; Tokunaga, F. *Biochemistry* **1996**, *35*, 14 047.
(14) Imamoto, Y.; Kataoka, M.; Tokunaga, F.; Asahi, T.; Masuhara, H. *Biochemistry* **2001**, *40*, 6047.
(15) Ujj, L.; Devanathan, S.; Meyer, T. E.; Cusanovich, M. A.; Tollin, G.; Atkinson, G. H. *Biophys. J.* **1998**, *75*, 406.
(16) Devanathan, S.; Pacheco, A.; Ujj, L.; Cusanovich, M.; Tollin, G.; Lin, S.; Woodbury, N. *Biophys. J.* **1999**, *77*, 1017.
(17) Hoff, W. D.; van Stokkum., I. H.; van Ramesdonk., H. J.; van Brederode., M. E.; Brouwer, A. M.; Fitch, J. C.; Meyer, T. E.; van Grondelle., R.; Hellingwerf, K. J. *Biophys. J.* **1994**, *67*, 1691.
(18) Gensch, T.; Gradinaru, C.; van Stokkum, I.; Hendriks, J.; Hellingwerf, K.; van Grondelle, R. *Chem. Phys. Lett.* **2002**, *356*, 347.
(19) Imamoto, Y.; Shirahige, Y.; Tokunaga, F.; Kinoshita, T.; Yoshihara, K.; Kataoka, M. *Biochemistry* **2001**, *40*, 8997.
(20) Brudler, R.; Rammelsberg, R.; Woo, T. T.; Getzoff, E. D.; Gerwert, K. *Nat. Struct. Biol.* **2001**, *8*, 265.
(21) Unno, M.; Kumauchi, M.; Sasaki, J.; Tokunaga, F.; Yamauchi, S. *Biochemistry* **2002**, *41*, 5668.
(22) Xie, A.; Kelemen, L.; Hendriks, J.; White, B. J.; Hellingwerf, K. J.; Hoff, W. D. *Biochemistry* **2001**, *40*, 1510.
(23) Ren, Z.; Perman, B.; Srajer, V.; Teng, T. Y.; Pradervand, C.; Bourgeois, D.; Schotte, F.; Ursby, T.; Kort, R.; Wulff, M.; Moffat, K. *Biochemistry* **2001**, *40*, 13 788.
(24) Genick, U. K.; Borgstahl, G. E.; Ng, K.; Ren, Z.; Pradervand, C.; Burke, P. M.; Srajer, V.; Teng, T. Y.; Schildkamp, W.; McRee, D. E.; Moffat, K.; Getzoff, E. D. *Science* **1997**, *275*, 1471.
(25) Unno, M.; Kumauchi, M.; Sasaki, J.; Tokunaga, F.; Yamauchi, S. *J. Am. Chem. Soc.* **2000**, *122*, 4233.
(26) Xie, A.; Hoff, W. D.; Kroon, A. R.; Hellingwerf, K. J. *Biochemistry* **1996**, *35*, 14 671.
(27) Genick, U. K.; Devanathan, S.; Meyer, T. E.; Canestrelli, I. L.; Williams, E.; Cusanovich, M. A.; Tollin, G.; Getzoff, E. D. *Biochemistry* **1997**, *36*, 8.
(28) Imamoto, Y.; Mihara, K.; Hisatomi, O.; Kataoka, M.; Tokunaga, F.; Bojkova, N.; Yoshihara, K. *J. Biol. Chem.* **1997**, *272*, 12 905.
(29) Meyer, T. E.; Cusanovich, M. A.; Tollin, G. *Arch. Biochem. Biophys.* **1993**, *306*, 515.
(30) Borucki, B.; Devanathan, S.; Otto, H.; Cusanovich, M. A.; Tollin, G.; Heyn, M. P. *Biochemistry* **2002**, *41*, 10 026.
(31) Meyer, T. E.; Tollin, G.; Hazzard, J. H.; Cusanovich, M. A. *Biophys. J.* **1989**, *56*, 559.

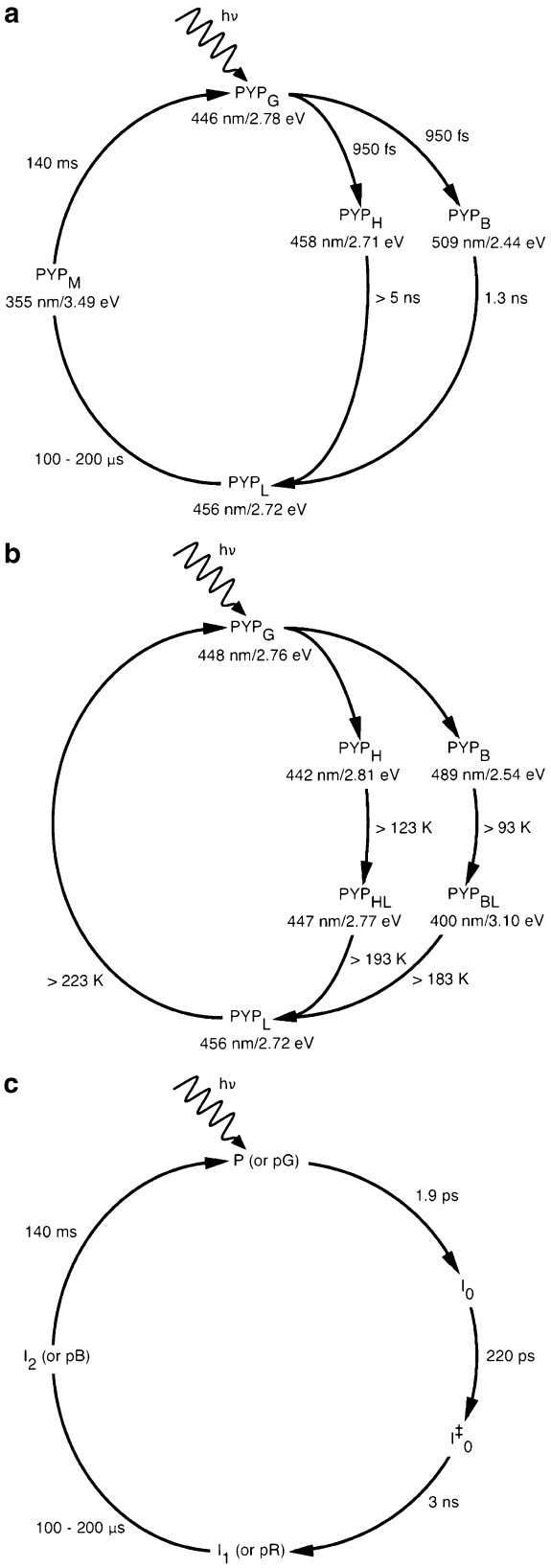

Figure 2. Photocycle intermediates observed by UV−vis spectroscopy (a,c) at room temperature with time-resolved techniques and (b) at low temperature with cryogenic trapping techniques. (a) and (c) depict alternative room-temperature photocycle kinetics reported by Imamoto et al.[14] and Devanathan et al.[16] respectively; with time constants for conversion between species. (b) depicts photocycle intermediates observed at low temperature;[13] with temperatures (K) of spontaneous (thermal) conversion between species. (a) and (b) provide λ_{max} (in nm) and equivalent excitation energy (in eV). (c) contains alternative nomenclature of Hoff et al.[17] in parentheses.

excitation energies with experimentally measured spectroscopic absorbances (λ_{max}). The time-dependent density functional theory (TDDFT) formalism is applied to calculate the excitation energies of the trans ($\theta = -180°$), transition state ($-90°$), and cis ($0°$) conformations along the isomerization pathway. Excitation energies are calculated and assignments are made for the two conformers reported in the single-crystal structure determined by Genick et al.[12] using cryogenic trapping techniques: the dark state (Figure 1b, green carbons) and an early intermediate state with $\theta = -80°$ (orange carbons), resulting from photoconversion of only 25% of the molecules in the crystal. This cryogenically trapped intermediate conformation was initially assigned to the PYP_{BL} intermediate based on an absorption spectrum measured in the frozen crystal which showed a 400 nm shoulder.[12] Now, this assignment is revised based on the correspondence of previously observed spectra with the calculations presented here. Comparison to previous computational work on PYP[33−35] are made, and the implications of our calculations for the photocycle mechanism of PYP are discussed.

2 Methods and Computational Details

2.1 Isomerization Calculations. Calculations to map out the electronic ground-state (S_0) surface over the isomerization coordinate were done for the isolated chromophore, deprotonated *para*-coumaryl methyl thioester (pCA-MT$^-$), and for a model of the PYP active site including that chromophore and chemical groups representing Tyr42, Glu46, Thr50, and Phe62 side chains (Figure 1a) taken from the dark state conformation in the 0.85 Å resolution crystal structure determined by Genick et al.[12] Tyr42 and Glu46 donate hydrogen bonds to the chromophore phenolate oxygen whereas Thr50 donates a hydrogen bond to the phenolic oxygen of Tyr42. Thr50 and Phe62 interact sterically with the chromophore, abutting both faces of the phenolic ring. The torsion angle about the central vinyl bond of pCA-MT$^-$ and the protein-bound chromophore ($\theta(C_4C_3C_2C_1)$ in Figure 1a) was taken as the isomerization coordinate. The first singlet excited state (S_1) energies were calculated as vertical excitations from selected points on the ground state (S_0) surface using time-dependent density functional theory (TDDFT).[36−39] These energies correspond approximately to the energies for electronic transitions from the highest occupied π to the lowest unoccupied π^* molecular orbital (HOMO → LUMO). The excitation energy calculations were performed using the Amsterdam Density Functional code (ADF2000.02).[40−42] The local density approximation (LDA) for the exchange and correlation were based on parametrization by Vosko, Wilk, and Nusair (VWN).[43] Generalized Gradient Approximations (GGA) were made using the Becke correction to exchange[44] and the Perdew correction to correlation.[45] The calculations

(32) Hoff, W.; Kwa, S.; van Grondelle, R.; Hellingwerf, K. *Photochem. Photobiol.* **1992**, *56*, 529.
(33) Molina, V. Merchan, M. *Proc. Natl. Acad. Sci. U.S.A.* **2001**, *98*, 4299.
(34) Sergi, A.; Gruning, M.; Ferrario, M.; Buda, F. *J. Phys. Chem. B* **2001**, *105*, 4386.
(35) Groenhof, G.; Lensink, M. F.; Berendsen, H. J. C.; Snijders, J. G.; Mark, A. E. *Proteins* **2002**, *48*, 202.
(36) Casida, M. E. In *Recent Advances in Density Functional Theory*; Chong, D. P., Ed.; World Scientific: Singapore, 1999; pages 100−110.
(37) Gross, E. Kohn, W. *Adv. Quantum Chem.* **1990**, *21*, 255.
(38) Gross, E.; Dobson, J.; Petersilka, M. *Density-Functional Theory of Time-Dependent Phenomena*; Springer: Heidelberg, 1996; pages 81−172.
(39) van Gisbergen, S.; Snijders, J.; Baerends, E. *Comput. Phys. Commun.* **1999**, *118*, 119.
(40) te Velde, G.; Bickelhaupt, F. M.; Baerends, E. J.; Guerra, C. F.; van Gisbergen, S. J. A.; Sniders, J. G.; Ziegler, T. *J. Comput. Chem.* **2001**, *22*, 931.
(41) Guerra, C. F.; Snijders, J. G.; te Velde, G.; Baerends, E. J. *Theor. Chem. Acc.* **1998**, *99*, 391.
(42) Scientific Computing Modelling NV. *ADF codes version 2000.02*. Department of Theoretical Chemistry, Vrije Universiteit, Amsterdam, **2000**.
(43) Vosko, S. H.; Wilk, L.; Nusair, M. *Can. J. Phys.* **1980**, *58*, 1200.

were done with triple-ζ Slater-type orbital (STO) basis sets, with a single set of polarization functions, which correspond to Basis Set IV in ADF.

The geometries used in the excitation energy calculations on the crystallographically observed intermediates (Figure 1b) had heavy atom positions taken directly from the high-resolution (0.85 Å) structure[12] and hydrogen positions optimized using ADF. The optimization of hydrogen positions is critical because the internuclear distance between the heavy atoms and hydrogens reported in the SHELX-refined crystal structure are shorter than a chemical bond length. Rather, the hydrogen nuclear positions used in the crystallographic refinement procedure are selected to optimally represent the hydrogen scattering[46,47] and must be optimized for reliable electronic structure calculations.

The geometry optimizations comprising the photoisomerization energy profile were performed using Gaussian 98 (revision A.7)[48] to exploit the superior optimization properties of the redundant internal coordinate system. We used the B3LYP hybrid functional composed of the exchange functional of Becke[44] and the correlation functional of Lee, Yang and Parr,[49] with atomic orbitals represented by the 6-31G* basis set. For the isolated chromophore, pCA-MT$^-$, the $\theta(C_4C_3C_2C_1)$ dihedral angle (Figure 1a) was stepped from 180° (trans) to 0° (cis) in 10° increments while all other degrees of freedom were optimized, except that the $\theta(H_3C_3C_2H_2)$ and $\theta(C_4C_3C_2C_1)$ dihedral angles about the central vinyl bond were constrained to be equal at each transit step.[50]

For the protein model, the geometries were obtained by a multistep procedure. First a coarse-grained optimization was performed, in which the $\theta(C_4C_3C_2C_1/H_3C_3C_2H_2)$ dihedral angle was stepped from −180° (trans) to 0° (cis) in 1° increments using the semiempirical PM3 Hamiltonian.[51] We computed the isomerization transit in both the $+\theta$ and $-\theta$ directions and determined that the potential energy curve is approximately symmetrical in our model (data not shown), meaning a more sophisticated model with additional protein residues would be required to determine energy differences for rotation in each direction. The $-\theta$ isomerization direction represents flipping of the carbonyl oxygen of the chromophore in the direction of Tyr98, and appears to involve fewer steric collisions.[12,52] The coordinates of residues T50 and F62 were constrained except for the hydroxyl proton of T50 (red atoms in Figure 1a are constrained). Protein residues Y42, E46 and the C69-bound chromophore were constrained at their terminal methylenes (β, γ, and α carbons, respectively). The atoms constrained in the PM3 isomerization transit exhibit little or no change in atomic positions between the two conformations observed in the cryogenically trapped crystal structure.[12]

Next, high-quality structures were computed along the isomerization transit from −180° (trans) to 0° (cis) in −10° increments by using the PM3 transit geometries in constrained optimizations with the ONIOM model of Morokuma et al.[53−55] The two-layer ONIOM model treated the chromophore (pCA-MT$^-$), Y42 and E46 using B3LYP/6-31G* and T50 and F62 using PM3 (Figure 1a). The protein residue (Y42, E46, T50, and F62) coordinates were constrained to their positions following the PM3 transit, except for the protons of the hydrogen bonds. The chromophore was constrained only at the position of the C_α methyl group. The T50 and F62 residues were excluded from the ground and excited-state energy calculations done using TDDFT in ADF (as described above).

2.2 Proton-Transfer Calculations. Potential-energy curves for the proton transfer from Glu46 to the chromophore were calculated for the dark state ($\theta = 162°$) and cryogenically trapped intermediate ($\theta = -80°$) structures of Genick, et al.[12] The geometries used heavy atom positions taken directly from the high-resolution structure and hydrogen positions optimized using ADF, as described for the excitation energy calculations above. The linear transit coordinate was from 0.7 Å from the Glu46 oxygen to 0.7 Å from the chromophore phenolate oxygen in approximately 0.05 Å steps. The proton-transfer calculations were done both in the gas phase and using the self-consistent reaction field (SCRF) model of the protein and solvent environment. SCRF calculations were done using ADF (as described above) for the quantum chemical atoms and the MEAD (Macroscopic Electrostatics with Atomic Detail)[56] suite of programs for the continuum electrostatic environment, in a procedure described previously.[57−61] The quantum mechanical atoms representing the chromophore, Y42 and E46 (Figure 1b) are embedded within a classical model of the low dielectric ($\epsilon = 2$) protein medium containing atom-centered PARSE charges and radii[62] for the remaining protein residues. The small protein dielectric ($\epsilon_{protein} = 2$) was determined to be appropriate for PYP due to its high thermal stability, based on pK_a calculations by Demchuk et al.[11] The protein region, delineated by the Connolly surface,[63] is further embedded within a high dielectric region ($\epsilon = 80$) representing water.

3 Results and Discussion

3.1 Photoisomerization Pathway. We calculated the potential energy curves (Figure 3) along the coordinate for isomerization about the $\theta(C_4C_3C_2C_1)$ torsion angle of the *para*-coumaryl methyl thioester (pCA-MT$^-$) chromophore, both in isolation and within the PYP active-site model illustrated in Figure 1a. Within the active-site model, which includes the steric interactions with residues T50 and F62 that restrain the plane of the chromophore ring, driving the torsion angle from trans → cis results in the anionic chromophore achieving the cis conformation by flipping its thioester carbonyl. We drove the isomerization in both the $+\theta$ and $-\theta$ directions. The $-\theta$ isomerization (Figure 3), which flips the carbonyl oxygen in the direction of Y98, appears to involve fewer steric collisions.[12,52] We observed that throughout the isomerization in either direction, the hydrogen bonds between the chromophore phenolic oxygen and Y42 and E46 were maintained, in accord with previous experimental results from time-resolved UV/

(44) Becke, A. D. *J. Chem. Phys.* **1986**, *84*, 4524.
(45) Perdew, J. P. *Phys. Rev. B* **1986**, *33*, 8822.
(46) Sheldrick, G. *SHELX-97 Manual* **1997**.
(47) Sheldrick, G.; Schneider, T. In *Methods in Enzymology*; Sweet, R. Carter Jr., C., Eds.; Academic Press: Orlando, Florida, 1997; Vol. 277, pages 319−343.
(48) Frisch, M. J.; Trucks, G. W.; Schlegel, H. B.; Scuseria, G. E.; Robb, M. A.; Cheeseman, J. R.; Zakrzewski, V. G.; Montgomery, J. A.; Jr.; Stratmann, R. E.; Burant, J. C.; Dapprich, S.; Millam, J. M.; Daniels, A. D.; Kudin, K. N.; Strain, M. C.; Farkas, O.; Tomasi, J.; Barone, V.; Cossi, M.; Cammi, R.; Mennucci, B.; an d C. Adamo, C. P.; Clifford, S.; Ochterski, J.; Petersson, G. A.; Ayala, P. Y.; Cui, Q.; Morokuma, K.; Malick, D. K.; Rabuck, A. D.; Raghavachari, K.; Foresman, J. B.; Cioslowski, J.; Ortiz, J. V.; Stefanov, B. B.; Liu, G.; Liashenko, A.; Piskorz, P.; Komaromi, I.; Gomperts, R.; Martin, R. L..; Fox, D. J.; Keith, T.; Al-Laham, M. A.; Peng, C. Y.; nayakkara, A. N.; Gonzalez, C.; Challacombe, M.; Gill, P. M. W.; Johnson, B.; Chen, W.; Wong, M. W.; Andres, J. L.; Gonzalez, C.; Head-Gordon, M.; Replogle, E. S.; Pople, J. A. *Gaussian 98* (Revision A.7), Gaussian, Inc., Pittsburgh, PA, 1998.
(49) Lee, C.; Yang, W.; Parr, R. *Phys. Rev. B* **1988**, *37*, 785.
(50) Han, W.; Lovell, T.; Liu, T.; Noodleman, L. *Chem. Phys. Chem.* **2002**, *3*, 167.
(51) Stewart, J. *J. Comput. Chem.* **1989**, *10*, 221.
(52) Getzoff, E. D.; Gutwin, K. N.; Genick, U. K. *Nat. Struct. Bio.* **2003**, submitted.
(53) Svensson, M.; Humbel, S.; Froese, R. D. J.; Matsubara, T.; Sieber, S.; Morokuma, K. *J. Phys. Chem.* **1996**, *100*, 19 357.
(54) Dapprich, S.; Komaromi, I.; Byun, K. S.; Morokuma, K.; Frisch, M. J. *J. Mol. Struct. (THEOCHEM)* **1999**, *461−462*, 1.
(55) Morokuma, K.; Musaev, D. G.; Vreven, T.; Basch, H.; Torrent, M.; Khoroshun, D. V. *IBM J. Res. Dev.* **2001**, *45*, 367.
(56) Lim, C.; Bashford, D.; Karplus, M. *J. Phys. Chem.* **1991**, *95*, 5610.
(57) Chen, J.; Noodleman, L.; Case, D.; Bashford, D. *J. Phys. Chem.* **1994**, *98*, 11 059.
(58) Li, J.; Nelson, M.; Peng, C.; Bashford, D.; Noodleman, L. *J. Phys. Chem. A* **1998**, *102*, 6311.
(59) Liu, T.; Ullmann, G. M.; Noodleman, L. SCRF 2000: A self-consistent-reaction-field code for use with ADF 2000, Jan., 2001.
(60) Thompson, M. J.; Liu, T.; Bashford, D.; Getzoff, E. D.; Noodleman, L. **2002**, in preparation.
(61) Asthagiri, D.; Dillet, V.; Liu, T.; Noodleman, L.; Van Etten, R. L.; Bashford, D. *J. Am. Chem. Soc.* **2002**, *124*, 10 225.
(62) Sitkoff, D.; Sharp, K.; Honig, B. *J. Phys. Chem.* **1994**, *98*, 1978.
(63) Connolly, M. *J. Appl. Crystallogr.* **1983**, *16*, 548.

Table 1. Excitation Energies (in eV[a]) Calculated for the PYP Chromophore in the Active-Site Model of Figure 1, and Compared With Spectroscopically Determined Intermediates

model[b]	E_{ex}[c]	f[d]	transition	E_{ex}(exp)[e]	intermediate[f]	translation[g]
$X_{(\theta = 162)}$	3.117 (0.000)	0.935	$\pi \rightarrow \pi^*$	2.78 (0.00)	PYP_G	P, pG
$S_{(\theta = -180)}$	3.049 (−0.068)	1.019	$\pi \rightarrow \pi^*$			
$S_{(\theta = -90)}$	0.089 (−3.028)	$<10^{-4}$	Figure 5a			
$X_{(\theta = -80)}$						
Chr $^-$, Glu ^{0}	2.401 (−0.716)	0.148	Figure 5b			
	2.636 (−0.481)	0.309	Figure 5b			
	2.743 (−0.374)	0.176	Figure 5c	2.44 (−0.34)	PYP_B (298 K) [h]	I_0, $I_0^{\ddagger}$
Chr ^{0}, Glu $^-$	0.497 (−2.620)	0.040	$n \rightarrow \pi^*$			
	2.866 (−0.251)	0.484	Figure 5d	2.54 (−0.24)	PYP_B (77 K) [i]	$I_0^{\ddagger}$
Chr ^{0}, Glu ^{0}	3.163 (0.046)	0.529	$\pi \rightarrow \pi^*$			
$S_{(\theta = 0)}$						
Chr $^-$, Glu ^{0}	3.037 (−0.080)	0.879	$\pi \rightarrow \pi^*$	2.67 (−0.11)	PYP_L	I_1, pR
Chr ^{0}, Glu $^-$	3.160 (0.043)	0.263	Figure 5e			
	3.188 (0.071)	0.346	Figure 5e			
	3.481 (0.364)	0.122	Figure 5f	3.10 (0.32)	PYP_{BL}	

[a] eV = 1239.6/nm. [b] Geometries from simulated model (S, this work), crystal structure (X, Genick et al.,[12] Protein Data Bank code 3PYP). Isomerization dihedral angle (θ). Chromophore (Chr) and E46 (Glu) ionization state. For $X_{\theta = 162}$, $S_{\theta = -180}$, and $S_{\theta = -90}$, the Chr-,Glu0 tautomer was used. [c] Only mechanistically relevant and high oscillator strength (spectroscopically observable) excitations are reported. Numbers in parentheses are shifts with respect to $X_{\theta = 162}$. [d] Oscillator strength. [e] Experimentally determined excitation energies[13,14] (conversion from λ_{max}). Numbers in parentheses are shifts with respect to PYP_G. [f] Assignment of structure or computational model to spectroscopic intermediate. [g] Alternative nomenclature for intermediate (see also Figure 2). [h] Time-resolved spectroscopy. [i] Cryogenically trapped intermediate.

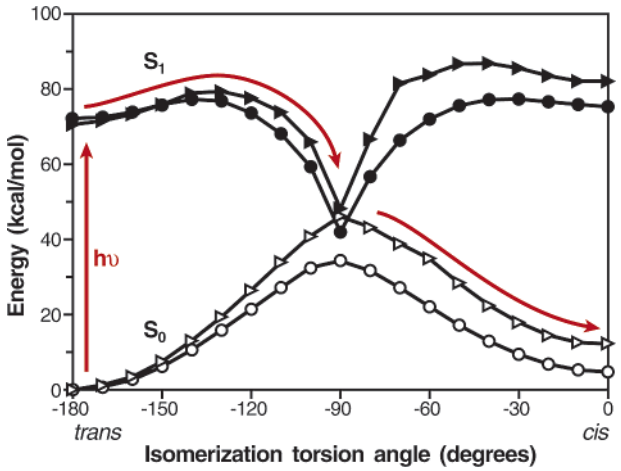

Figure 3. Potential energy curves for isomerization of pCA-MT$^-$, both isolated (circles) and within the PYP active site, including Tyr42 and Glu46 (right-facing triangles). Excited-state singlet (S_1, filled symbols) calculations were done using TDDFT vertical excitations from ground state (S_0, open symbols) constrained optimizations. The reaction coordinate is over isomerization of the dihedral angle $\theta(C_4C_3C_2C_1)$ shown in Figure 1. The photocycle pathway taken by the system is shown in red arrows, representing photoexcitation, isomerization and internal conversion.

visible spectroscopy of the E46Q mutant,[64] Fourier transform infrared (FTIR) and Raman spectroscopy,[19−21] and X-ray crystallography.[12,23]

The transition state barrier at $\theta = -90°$ along the ground-state surface (S_0 in Figure 3) is 12 kcal/mol higher in energy for the protein model (46 kcal/mol) than the free chromophore (34 kcal/mol) because of the conformational strain (e.g., the subtle bowing of the chromophore) associated with isomerizing within the protein. However, both barriers are well below the 64 kcal/mol provided by the absorbed photon (446 nm). The ground-state energy of the $\theta = 0°$ (cis) conformation in the protein active site is 7 kcal/mol higher than the cis conformation of isolated pCA-MT$^-$, due primarily to a 17° increase in the $C_{methyl}-S-C_4$ bond angle coupling the chromophore and C69 residue of the protein and to an 11° increase in the $S-C_4-C_3$ bond angle. Both of these contribute to the stretch of the chromophore to maintain its hydrogen bonds with Y42 and E46. The $\theta = 0°$ conformation in the protein model is 12 kcal/mol higher than the −180° conformation, both because of these bond angle increases and because of the steric clash between the carbonyl oxygen and a ring hydrogen on the chromophore. This 12 kcal/mol energy difference represents the potential energy available to complete the photocycle via thermal fluctuations.

The excited-state potential energy curves for the isolated chromophore and protein model (S_1 in Figure 3) were calculated as vertical excitations from the ground-state surface using TDDFT. The calculated $\pi \rightarrow \pi^*$ excitation energy of the idealized trans planar conformation in the protein model (3.05 eV, $S_{\theta = -180}$ in Table 1) compares well with PYP_G (2.78 eV, 446 nm). The excitation energy of the dark state conformation ($X_{\theta = 162}$) calculated from the crystal structure[12] (3.12 eV) was slightly blue-shifted (0.07 eV) due to deviation from planarity (bowing and twisting of the chromophore) which affects the $\pi \rightarrow \pi^*$ transition. A visual representation of the calculated transition superimposed on the spectroscopic absorbance data[15] is provided in Figure 4. The blue bar in that figure represents the calculated excitation energy of the dark state conformation from the crystal structure, and has been shifted to the peak of the P (or PYP_G) spectroscopic intermediate as in Table 1 to aid in the assignment of atomic structures to later photocycle intermediates. The solvatochromatic shift due to the effects of the protein environment (conformational strain, protein and solvent medium screening, hydrogen bonding) on the excitation energy of the dark state chromophore has been studied extensively.[34,60,65−67]

The chromophore isomerization from −180° to −90° along the S_1 surfaces (Figure 3) overcomes an apparent calculated activation barrier of approximately 9 kcal/mol. However, the excited-state potential energy surface depicted is for vertical excitation, while the "true" surface would allow for adiabatic relaxation as a function of θ. This barrier is higher than the 5 kcal/mol barrier calculated for the free pCA-MT$^-$ chromophore. At the −90° conformation, the energy gap between the ground

(64) Devanathan, S.; Lin, S.; Cusanovich, M. A.; Woodbury, N.; Tollin, G. *Biophys. J.* **2000**, *79*, 2132.

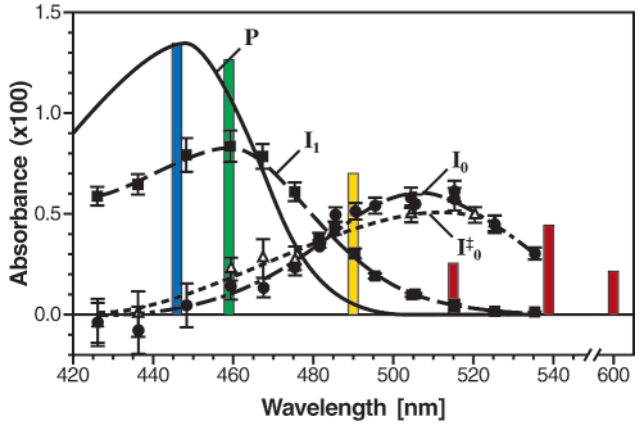

Figure 4. Assignment of calculated excitation energies (bars) to spectroscopically determined absorbances[15] (background data). Blue bar is dark state conformation from Genick et al. crystal structure.[12] Green bar is cis (0°) conformation from the modeled photoisomerization pathway (Figure 3). Yellow bar is cryogenically trapped conformation from crystal structure[12] with chromophore protonated. Red bars are three observable transitions for cryogenically trapped conformation from crystal structure[12] with anionic chromophore (Glu46 protonated). Calculated excitation energies (in eV; Table 1) converted to wavelengths (nm). Position of bars relative to assignment of the dark state conformation to the P intermediate.

and excited states was calculated at 2 kcal/mol within the protein and 8 kcal/mol in pCA-MT$^-$, both with near-zero oscillator strength ($S_{\theta\,=\,-90}$ in Table 1) as expected for an internal conversion process.[68] The molecular orbitals involved in the internal conversion are shown in Figure 5a, where the π densities of the HOMO (orange) and LUMO (blue) are in nearly orthogonal planes, giving a near-zero value for the transition dipole moment matrix element (almost dipole forbidden). In the internal conversion process, the electron relaxes from the excited-state orbital on the phenolate ring and C_2 of the isomerizing bond (Figure 1a) to the ground-state orbital on the C_3 of the isomerizing bond and the chromophore carbonyl group.

The excitation energy calculated for the modeled cis conformer in the protein is 3.04 eV ($S_{\theta\,=\,0}$[Chr$^-$,Glu^0] in Table 1). In assigning simulated (S) and crystallographic (X) structures to spectroscopically observed intermediates, we compare shifts in excitation energies (values in parentheses in Table 1; colored bars in Figure 4) relative to an assignment of the dark state structure[12] (Figure 1b, green atoms) to PYP_G (blue bar in Figure 4). In general, we consider the calculated spectral shifts with respect to dark state to be more reliable than the absolute excitation energy predictions. By that criterion, the $\theta = 0°$ model corresponds well with the nanosecond intermediate, PYP_L or I_1 (Table 1; green bar in Figure 4). Previous computational studies by Sergi et al.[34] had shown that manually flipping the carbonyl group of the chromophore to create a model of PYP_L also gives an excitation energy which matches that intermediate.

Another previous computational study by Groenhof et al.[35] had used classical molecular dynamics simulations to model the isomerization of the chromophore in PYP. However, the conformation observed following isomerization was said to resemble that of the time-resolved Laue X-ray diffraction structure of the PYP_L intermediate by Perman et al.,[69] which is characterized by a highly strained chromophore conformation with a pseudo-sp^3 hybridized carbonyl carbon (C_4 in Figure 1a) and a broken hydrogen bond between the chromophore phenolate oxygen and Glu46. That crystal structure has since been revised by those authors[23] to one in which the chromophore achieves the isomerization by flipping its carbonyl group. The revised interpretation is in better agreement with the electron density determined crystallographically, and addresses concerns with the disagreement between the original structure and FTIR and UV−vis spectroscopic data.[20,33]

We have not attempted to model the chromophore isomerization within the protein active site beyond the PYP_L intermediate because the protein has been shown by NMR,[70,71] FTIR,[72] and circular dichroism (CD) spectroscopy,[73] and by mutational studies[74] and molecular dynamics simulations[75,76] to exhibit significant dynamical flexibility on rearrangement to PYP_M. Thus, the later photocycle steps likely follow a complicated reaction coordinate more suitably examined using other methods than those described here.

3.2 Proton-Transfer Calculations. Energy surfaces for proton transfer across the buried hydrogen bond between Glu46 and the chromophore were determined for the dark state (PYP_G) and cryogenically trapped intermediate ($X_{\theta\,=\,-80}$) conformations of the crystal structure[12] (Figure 1b). In the case of the dark state, protonated Glu46 is the favored state (Figure 6a, dotted line). In the cryogenically trapped ($X_{\theta\,=\,-80}$) intermediate conformation, the Glu46-chromophore oxygen−oxygen distance is increased to 2.77 Å compared with 2.61 Å in the dark state structure ($X_{\theta\,=\,162}$); and protonated Glu46 is still the favored state, but a broad shoulder develops in the coordinate range corresponding to protonation of the chromophore (Figure 6a, solid line). The energy surface for proton transfer in the 0° (cis) model (PYP_L, not shown) is nearly identical to that of the dark state structure. Previous efforts to study proton transfer in the PYP_L intermediate have been made;[76] however, those calculations were based on an incorrect crystallographic model[69] which has since been revised as described above.

To examine the effects of the rest of the protein and the solvent, SCRF calculations, in which these effects are modeled by continuum electrostatics (see methods), were also used to model the proton transfer. When the dark state conformation is examined using the SCRF approach, the protonation of Glu46 is favored by approximately 12 kcal/mol (Figure 6b, dotted line), compared with 17 kcal/mol in the gas phase calculations. The decreased energy difference between the two protonation states in the SCRF calculations is due to screening by the protein and

(65) Thompson, M. J.; Liu, T.; Bashford, D.; Getzoff, E. D.; Noodleman, L. **2002**, in preparation.
(66) Imamoto, Y.; Koshimizu, H.; Mihara, K.; Hisatomi, O.; Mizukami, T.; Tsujimoto, K.; Kataoka, M.; Tokunaga, F. *Biochemistry* **2001**, *40*, 4679.
(67) Yoda, M.; Houjou, H.; Inoue, Y.; Sakurai, M. *J. Phys. Chem. B* **2001**, *105*, 9887.
(68) Turro, N. J. *Modern Molecular Photochemistry*; University Science Books: Sausalito, California, 1991; chapter 1−6.
(69) Perman, B.; Srajer, V.; Ren, Z.; Teng, T.; Pradervand, C.; Ursby, T.; Bourgeois, D.; Schotte, F.; Wulff, M.; Kort, R.; Hellingwerf, K.; Moffat, K. *Science* **1998**, *279*, 1946.
(70) Rubinstenn, G.; Vuister, G. W.; Mulder, F. A.; Dux, P. E.; Boelens, R.; Hellingwerf, K. J.; Kaptein, R. *Nat. Struct. Biol.* **1998**, *5*, 568.
(71) Craven, C. J.; Derix, N. M.; Hendriks, J.; Boelens, R.; Hellingwerf, K. J.; Kaptein, R. *Biochemistry* **2000**, *39*, 14 392.
(72) Hoff, W. D.; Xie, A.; Van Stokkum., I. H.; Tang, X. J.; Gural, J.; Kroon, A. R.; Hellingwerf, K. J. *Biochemistry* **1999**, *38*, 1009.
(73) Ohishi, S.; Shimizu, N.; Mihara, K.; Imamoto, Y.; Kataoka, M. *Biochemistry* **2001**, *40*, 2854.
(74) van der Horst, M. A.; van Stokkum., I. H.; Crielaard, W.; Hellingwerf, K. J. *FEBS Lett.* **2001**, *497*, 26.
(75) Shiozawa, M.; Yoda, M.; Kamiya, N.; Asakawa, N.; Higo, J.; Inoue, Y.; Sakurai, M. *J. Am. Chem. Soc.* **2001**, *123*, 7445.
(76) Groenhof, G.; Lensink, M. F.; Berendsen, H. J. C.; Mark, A. E. *Proteins* **2002**, *48*, 212.

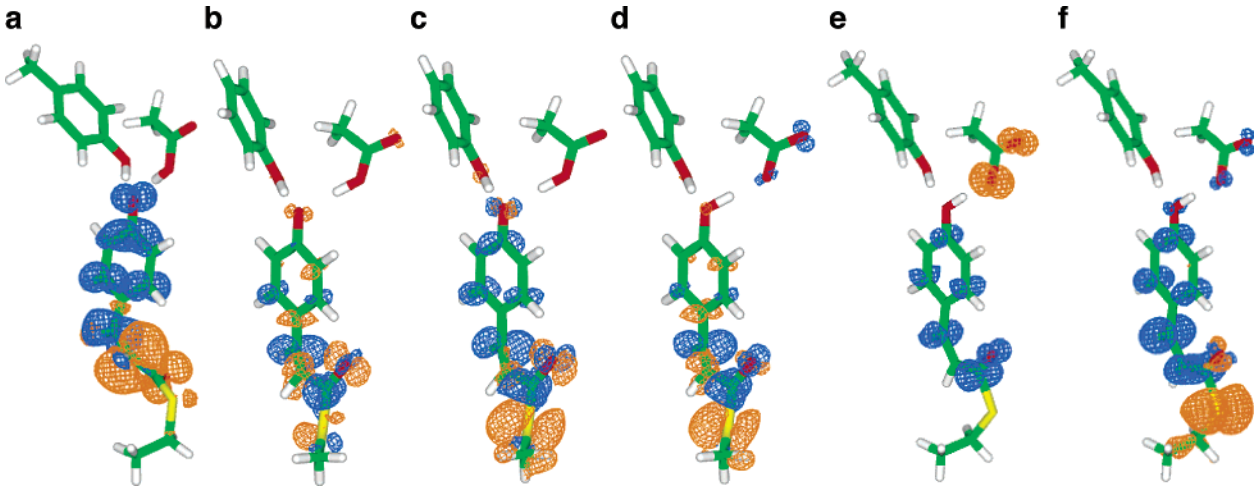

Figure 5. Calculated difference electron density due to electronic excitation (The electron density is reported as the difference between the density following and prior to the TDDFT-calculated transition. Both the ground state and the excited state may involve more than one Kohn−Sham (KS) orbital, in which case the density is taken as a sum of the KS orbital densities weighted by the fractional contribution of each to the calculated transition.) The excess electron density for the originating molecular orbital(s) are shown in orange contours and for the resultant orbital(s) are shown in blue contours. Transitions are shown for (a) the modeled-90° state, (b−c) the cryogenically trapped crystallographic intermediate with E46 protonated, (d) the cryogenically trapped intermediate with the chromophore protonated, and (e−f) the modeled 0° state with the chromophore protonated. The transitions are referenced to structures and excitation energies listed in Table 1.

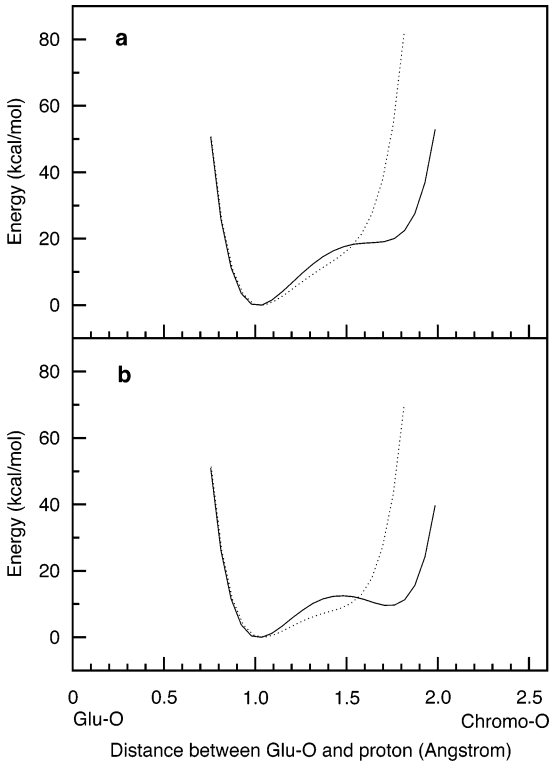

Figure 6. Energy surface for proton transfer from Glu46 oxygen (at origin) to the chromophore phenolate oxygen for the structurally determined photocycle intermediates (Figure 1b) in gas phase (a) and protein SCRF (b) calculations. Energies referenced to 0 kcal/mol at proton equilibrium position, approximately 1.0 Å from Glu46 oxygen. For both (a) and (b), the dotted curve is the dark state, PYP_G, and the solid curve is the cryogenically trapped intermediate (Figure 1b, orange atoms). The Glu−O···Chromophore−O distance changes from 2.61 Å in the dark state to 2.77 Å in the cryogenically trapped intermediate.

water medium, which makes localization of negative charge on the glutamate carboxyl less unfavorable. Repeating the SCRF calculation with the protein charges set to zero reveals an identical energy profile, confirming that solvent screening, and not the specific protein charges, is responsible. This effect is even more pronounced in the cryogenically trapped intermediate (Figure 6b, solid line). Due to the increased hydrogen bond length in that structure, the inclusion of solvent effects results in the appearance of a second well for protonation of the chromophore. The energy barrier to proton transfer from Glu46 to the chromophore is 12 kcal/mol in the forward direction and 3 kcal/mol in the reverse direction.

These calculations neglect some features of the proton transfer reaction in favor of a simple model: (1) vibrational effects, particularly the zero point energy but also coupled protein-chromophore vibrations. The inclusion of zero point energy effects, which can be significant for O−H bonds, would be expected to reduce the effective barrier to proton transfer by at least 3−5 kcal/mol. (2) Proton tunneling, which would also facilitate proton transfer. Even with the more simple model, our calculations show the feasibility of proton transfer to the chromophore in the cryogenically trapped intermediate of Genick et al.[12]

3.3 Assignment of Structural to Spectroscopic Intermediates. The primary goal of this work is to develop a complete model of the early stages of the PYP photocycle (from PYP_G to PYP_L) by reconciling previous structural and spectroscopic studies through computational studies. The isomerization energy profile reported here (Figure 3) did not show stable intermediates between PYP_G and PYP_L, presumably because of the limited protein environment included in this computationally intensive model. To study the early photocycle intermediates, the excitation energy of the cryogenically trapped intermediate[12] (Figure 1b, orange carbons) was determined, assuming an anionic chromophore and protonated glutamic acid (Glu46). Three excitations within the visible spectrum (2.40, 2.64 and 2.74 eV; $X_{\theta\ =\ -80}[Chr^-,Glu^0]$ in Table 1; red bars in Figure 4) were shown to have significant oscillator strengths, meaning they have a large enough extinction coefficient to be spectroscopically observable. The highest energy of those excitations corresponds closely (when examining shifts with respect to PYP_G) with the λ_{max} of the picosecond room-temperature intermediates PYP_B (509 nm), determined by Imamoto et al.,[14] and I_0 (510 nm),

determined by Ujj et al.[15] The time-resolved spectra of PYP_B and I_0 reveal very broad absorbance profiles (from 480 nm to beyond 550 nm), in agreement with the additional lower energy excitations calculated here and with the presence of a higher-energy absorbing sub-population (described below).

Previous work using complete active space (CAS-type) quantum chemical calculations[33] assigned the cryogenically trapped crystal structure to the PYP_{HL} intermediate observed only at low temperature.[14] We believe this assignment is incorrect because the chemical model used in that study (1) included only the chromophore, neglecting electrostatic polarization and charge transfer effects due to the hydrogen bonding residues Tyr 42 and Glu46, and (2) took proton positions directly from the crystal structure.[77] As discussed in the methods section, the heavy atom-hydrogen bond lengths from the crystal structure are not accurate internuclear distances. Test calculations with TDDFT on their models of the dark state and cryogenically trapped intermediate show a pattern of excitation energies that would be complicated to interpret and does not match any spectroscopically observed intermediate before PYP_L. (Excitation energies for pCA-MT^- with short proton distances were calculated for the dark state (2.931 (0.000) eV, $f = 0.825$) and cryogenically trapped (1.208 (-1.723) eV, $f = 0.052$; 2.327 (-0.604) eV, $f = 0.136$; 2.814 (-0.117) eV, $f = 0.226$) conformations. Energy shifts (in parentheses) do not match known intermediates before PYP_L.) Additionally, Molina et al.[33] observed a low-energy (1.24 eV) excitation for this intermediate and proposed spectroscopic experiments probing absorbance in the 800−1000 nm region for its identification. In our model with the hydrogen positions optimized and the quantum cluster containing Tyr42 and Glu46 (Figure 1b; orange carbon atoms), that low-energy transition becomes significantly blue-shifted and possesses negligible oscillator strength relative to test calculations on their model.

We also performed TDDFT calculations on the cryogenically trapped intermediate with a protonated chromophore and deprotonated Glu46, an ionization state ignored in previous calculations. This model ($X_{\theta = -80}[Chr^0,Glu^-]$ in Table 1; yellow bar in Figure 4) shows a higher energy excitation of 2.87 eV (with high oscillator strength, $f = 0.48$), corresponding closely with experimental measurements for PYP_B at liquid nitrogen temperature.[13] The possibility of chromophore protonation in the PYP_B intermediate was discussed briefly by Imamoto et al.[19] because of the presence of some low-temperature FTIR spectral bands indicative of chromophore protonation. However, they ruled out that ionization state on the assumption that chromophore protonation must result in blue-shifting relative to the 446 nm dark state absorption, and because IR spectral bands indicating Glu46 protonation were observed in the same samples. In contrast, our calculations show that the proton transfer need not result in a blue shift relative to the dark state, and that the observed bands could be accounted for by a mixture of two ionization states in their low-temperature sample.

At room temperature, a similar mixture of two ionization states aids interpretation of the picosecond time-resolved spectra. The protonated chromophore (Chr^0,Glu^-) state would explain the high-energy shoulder of the PYP_B spectrum[14] and distinguish the two 510 nm species, I_0 and $I_0^{\ddagger}$, of Ujj et al.[15] The $I_0^{\ddagger}$ spectrum (Figure 4) exhibits enhanced absorptivity at 490 nm compared with I_0, consistent with a sub-population of proteins containing a protonated chromophore. The molecular orbitals involved in the excitation of $X_{\theta = -80}[Chr^0,Glu^-]$ (Figure 5d) resemble those of the deprotonated chromophore in the same intermediate (Figures 5b−c), indicating that the broad electronic excitation spectrum[14,15] may be due not only to subtle shifts in density but also to the proton position. These results, as well as the proton-transfer calculations described above, would indicate the feasibility of rapid proton exchange between the chromophore and Glu46 in this structural intermediate (PYP_B).

The details of the crystal structure[12] itself also support considerable chromophore protonation in the cryogenically trapped intermediate. The structure was determined at such high resolution (0.85 Å) that each atom could be individually refined without restraints to idealized geometries, allowing for accurate bond length determination. Light excitation of the cryogenically cooled crystal resulted in only a proportion of the protein molecules initiating the photocycle, giving partial occupancy of both the dark state and the early-intermediate structure in the same crystal. The C−O bond lengths for the dark state Glu46 carboxylate were 1.32 and 1.22 Å for the protonated and unprotonated oxygens, respectively, while for the cryogenically trapped intermediate they changed to 1.27 and 1.24 Å, and do not clearly indicate protonation of Glu46.

Calculations were also done on the protonated chromophore (Chr^0, Glu^-) ionization state of the 0° (cis) model, whose (Chr^-, Glu^0) protonation state we have identified with the PYP_L intermediate (see above). Three high-energy transitions with significant oscillator strengths were observed (3.16, 3.19, and 3.48 eV; $S_{\theta = 0}[Chr^0,Glu^-]$ in Table 1). The two lower energy transitions involve excitation from the Glu46 π molecular orbital to the π^* molecular orbital on the chromophore (Figure 5e). The highest energy transition is primarily from a *p* atomic orbital on the chromophore sulfur to the π^* LUMO on the chromophore (Figure 5f), the energy of which closely matches the λ_{max} of the strongly blue-shifted low-temperature intermediate, PYP_{BL} (Table 1). Protonation of the chromophore in PYP_{BL} is consistent with continuation of the low-temperature photocycle from a protonated chromophore in PYP_B (Figure 2b). By contrast, it is known from FTIR studies[19,20,22] that the PYP_L intermediate is deprotonated at the chromophore phenolate, and the present proton-transfer calculations show that chromophore protonation in the 0° (cis) model is energetically unfavorable (data similar to PYP_G; dotted lines in Figure 6). However, as in the case of the cryogenically trapped intermediate, increasing the glutamate oxygen-chromophore oxygen bond distance would likely result in a discrete well for proton localization at the chromophore phenolate. Increasing this distance would also eliminate the contribution of the two lower energy transitions (3.16 and 3.19 eV) to the visible spectrum because they involve significant electron density from Glu46, leaving the transition matching the experimentally observed PYP_{BL} absorbance maximum. For these reasons, we speculate that the PYP_{BL} intermediate is a protonated, cis (0°) chromophore inside the protein active site, with an increased chromophore-Glu46 hydrogen bond distance. The chromophore in this intermediate would be expected to relax to the PYP_L conformation and transfer its proton back to Glu46. This discussion is consistent with results showing that the PYP_{BL} intermediate is not observed at room temperature, where PYP_B relaxes directly to PYP_L.[14]

(77) Molina, V. Merchan, M. personal communication, 2002.

4 Conclusions

One challenge faced in molecular biophysics research is to reconcile results from different experimental techniques to determine mechanism. In the case of the photoactive yellow protein, this means comparing the results from a myriad of spectroscopic and structural studies done over many scales of time and at different temperatures. We have shown here that computational chemistry can help to resolve questions and apparent conflicts arising from experimental photobiology. Before this study, the structures of the spectroscopically determined early photocycle intermediates were unknown and questions were raised about the early intermediate structure of Genick et al.[12] being an artifact of the cryogenic trapping technique used in its determination. We have shown here that the assignment of that early intermediate crystal structure to the PYP_B intermediate resolves many questions arising from the spectroscopic studies. For instance, the difference in the λ_{max} of PYP_B at low temperature and at room temperature is explained by proton exchange between the chromophore and Glu46, as are the complicated low-temperature FTIR spectra of that intermediate.[19] Additionally, linear transit calculations are used to produce models for the structures of the PYP_{BL} and PYP_L intermediates. Even though the chromophore is deprotonated in both the PYP_G and PYP_L intermediates, we have shown that it is incorrect to assume that proton transfer from Glu46 does not play a role in intervening intermediates (PYP_B and PYP_{BL}).

On the basis of this work, we present a clarified picture of the early steps in the PYP photocycle observed at room temperature. Photoabsorption by the deprotonated, trans chromophore in the dark state (PYP_G, P, or pG) produces an excited state in which isomerization about the central vinyl bond (θ-($C_4C_3C_2C_1$)) of the chromophore is facilitated. The isomerization occurs by flipping the carbonyl linkage to the protein while maintaining hydrogen bonds between the chromophore phenolate and protein residues Tyr42 and Glu46. After crossing the transition state barrier, relaxation from the excited state to the ground state by internal conversion yields the first thermally stable photocycle intermediate, PYP_B (or I_0). This intermediate corresponds to the cryogenically trapped conformation ($\theta = -80$) in the structure determined by Genick et al.[12] The chromophore is predominantly in the deprotonated form in PYP_B, although a sub-population of the protonated chromophore species explains both the low temperature (77 K) blue shifted absorbance (489 nm) and the increased absorptivity at 490 nm in the $I_0^{\ddagger}$ intermediate observed at room temperature. The photoisomerization proceeds to form a deprotonated, cis chromophore in which the hydrogen bonds to Tyr42 and Glu46 are maintained, known as the PYP_L (or I_1; pR) intermediate. Going forward, we expect that computation will play a major role in resolving questions about the later steps in the PYP photocycle, currently the focus of active investigation.

Acknowledgment. This work was supported by NIH grants GM45607 (D.B.), GM43278 (L.N.), and GM37684 (E.D.G.); M.J.T. was supported by predoctoral fellowships from the La Jolla Interfaces in Science and the Skaggs Institute for Chemical Biology. We thank Dilip Asthagiri, Ronald Brudler, Ulrich K. Genick, Tim Lovell, Fahmi Himo, and Wen-ge Han for helpful discussions, and Tiqing Liu and Matthias Ullmann for use of the latest SCRF2000 code.

JA0294461